Brief Report

Cell Stem Cell

Genetic Ablation of *AXL* Does Not Protect Human Neural Progenitor Cells and Cerebral Organoids from Zika Virus Infection

Graphical Abstract

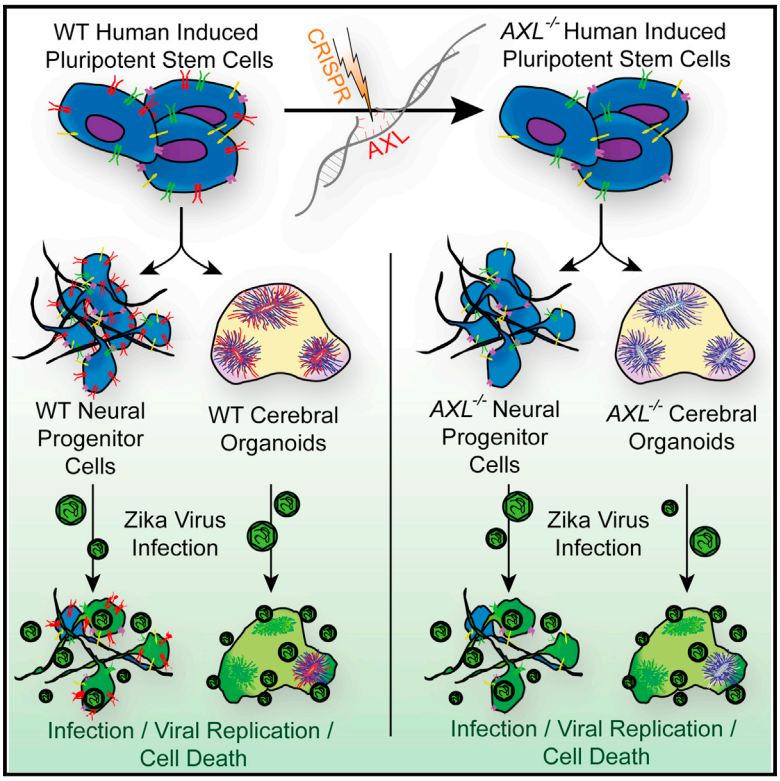

Authors

Michael F. Wells, Max R. Salick, Ole Wiskow, ..., Chaoyang Ye, Ajamete Kaykas, Kevin Eggan

Correspondence

ajamete.kaykas@novartis.com (A.K.), eggan@mcb.harvard.edu (K.E.)

In Brief

Wells et al. investigated ZIKV infection in neural cell types harboring deletions of the human AXL gene. Loss of this candidate ZIKV attachment factor had no effect on infectivity or virus-mediated cell death in neural progenitors or cerebral organoids, suggesting that AXL-independent mechanisms are prominent in these cells.

Highlights

- ZIKV can infect and kill AXL-knockout human neural progenitor cells
- Wild-type and AXL-knockout cerebral organoids display similar decreases in 2D area
- Candidate ZIKV attachment factor *TYRO3* is also expressed in neural progenitor cells
- Further studies are needed to identify key viral entry receptors in neural progenitors

Wells et al., 2016, Cell Stem Cell *19*, 703–708
December 1, 2016
http://dx.doi.org/10.1016/j.stem.2016.11.011

CellPress

Cell Stem Cell
Brief Report

Genetic Ablation of *AXL* Does Not Protect Human Neural Progenitor Cells and Cerebral Organoids from Zika Virus Infection

Michael F. Wells,[1,2,4] Max R. Salick,[3,4] Ole Wiskow,[2] Daniel J. Ho,[3] Kathleen A. Worringer,[3] Robert J. Ihry,[3] Sravya Kommineni,[3] Bilada Bilican,[3] Joseph R. Klim,[2] Ellen J. Hill,[2] Liam T. Kane,[2] Chaoyang Ye,[3] Ajamete Kaykas,[3,*] and Kevin Eggan[1,2,5,6,*]

[1]Stanley Center for Psychiatric Research, Broad Institute of MIT and Harvard, Cambridge, MA 02142, USA
[2]Department of Stem Cell and Regenerative Biology and Harvard Stem Cell Institute, Harvard University, Cambridge, MA 02138, USA
[3]Department of Neuroscience, Novartis Institutes for BioMedical Research, Cambridge, MA 02139, USA
[4]Co-first author
[5]Lead Contact
[6]Twitter: @EgganLab
*Correspondence: ajamete.kaykas@novartis.com (A.K.), eggan@mcb.harvard.edu (K.E.)
http://dx.doi.org/10.1016/j.stem.2016.11.011

SUMMARY

Zika virus (ZIKV) can cross the placental barrier, resulting in infection of the fetal brain and neurological defects including microcephaly. The cellular tropism of ZIKV and the identity of attachment factors used by the virus to gain access to key cell types involved in pathogenesis are under intense investigation. Initial studies suggested that ZIKV preferentially targets neural progenitor cells (NPCs), providing an explanation for the developmental phenotypes observed in some pregnancies. The AXL protein has been nominated as a key attachment factor for ZIKV in several cell types including NPCs. However, here we show that genetic ablation of *AXL* has no effect on ZIKV entry or ZIKV-mediated cell death in human induced pluripotent stem cell (iPSC)-derived NPCs or cerebral organoids. These findings call into question the utility of AXL inhibitors for preventing birth defects after infection and suggest that further studies of viral attachment factors in NPCs are needed.

Zika virus (ZIKV) is an enveloped single-stranded RNA virus in the flavivirus family. While 80% of adults present as asymptomatic when infected (Petersen et al., 2016), ZIKV can cause fever, rash, conjunctivitis, and more rarely Guillain-Barre Syndrome (Cao-Lormeau et al., 2016; Malkki, 2016; Oehler et al., 2014). Pregnant women are an especially vulnerable population (Petersen et al., 2016), with infection linked to fetal microcephaly (Mlakar et al., 2016; Rubin et al., 2016; Soares de Oliveira-Szejnfeld et al., 2016), intracranial calcifications (Brasil et al., 2016), and fetal death (Sarno et al., 2016).

Early reports have drawn possible links between ZIKV infection and microcephaly by investigating the cell tropism of the virus in vitro. ZIKV was found to preferentially target neural progenitor cells (NPCs) (Tang et al., 2016). Studies employing neurospheres and cerebral organoids have also demonstrated the susceptibility of NPCs and radial glia to infection (Cugola et al., 2016; Dang et al., 2016; Garcez et al., 2016; Qian et al., 2016). Similarly, direct infection of E15 mouse brain resulted in high concentrations of ZIKV in the radial-glia-rich ventricular zone, while parallel infections with the closely related West Nile Virus (WNV) showed increased tropism in neurons of the intermediate zone and cortical plate regions (Brault et al., 2016). It has been theorized that these variations in tropism could be explained in part by the differing expression profiles of the TYRO3-AXL-MERTK (TAM) family of receptors, which are hypothesized to be key attachment factors for ZIKV (Hamel et al., 2015; Nowakowski et al., 2016) and other enveloped viruses (Hunt et al., 2011; Meertens et al., 2012). Importantly, investigations using non-neuronal cell types have shown that ZIKV infectivity can be reduced by modulating AXL with siRNA knockdown, CRISPR/Cas9 deletion, or incubation with neutralizing antibodies (Hamel et al., 2015; Savidis et al., 2016). Though the evidence implicating AXL in ZIKV pathogenesis is mounting, the role of AXL in ZIKV entry and cell death in human NPCs has yet to be directly tested. We therefore investigated whether targeted disruption of *AXL* in stem cells, followed by their differentiation, would result in NPCs resistant to ZIKV infection.

To allow rapid deletion of AXL in stem cells, we first inserted doxycycline-inducible Cas9 (dox-iCas9) into the AAVS1 locus of a human induced pluripotent stem cell (iPSC) line via TALENs (Figures S1A and S1B). CRISPR targeting RNAs (crRNAs) were then designed to target ubiquitously expressed exons within *AXL* (Figure S1C, Table S1). Cas9 induction, along with transfection of crRNAs and *trans*-activating CRISPR targeting RNA (tracrRNA), led to successful editing (T7E1; Figure S1D). crRNAs that targeted exons encoding the transmembrane domain (gRNA-Tm) and the extracellular domain (gRNA-Ec) were found to be the most efficient at editing, and were thus selected and used for human iPSC editing. Next-generation sequencing of these target regions from the resulting stem cells revealed that most alleles harbored frameshift mutations (Figure S1E, Table S2). iPSCs containing no *AXL* mutations, transmembrane-exon mutations, or extracellular-exon mutations were designated AXL^{WT}, $AXL^{KO\text{-}Tm}$, and $AXL^{KO\text{-}Ec}$, respectively. Edited cell lines remained pluripotent and had normal karyotypes.

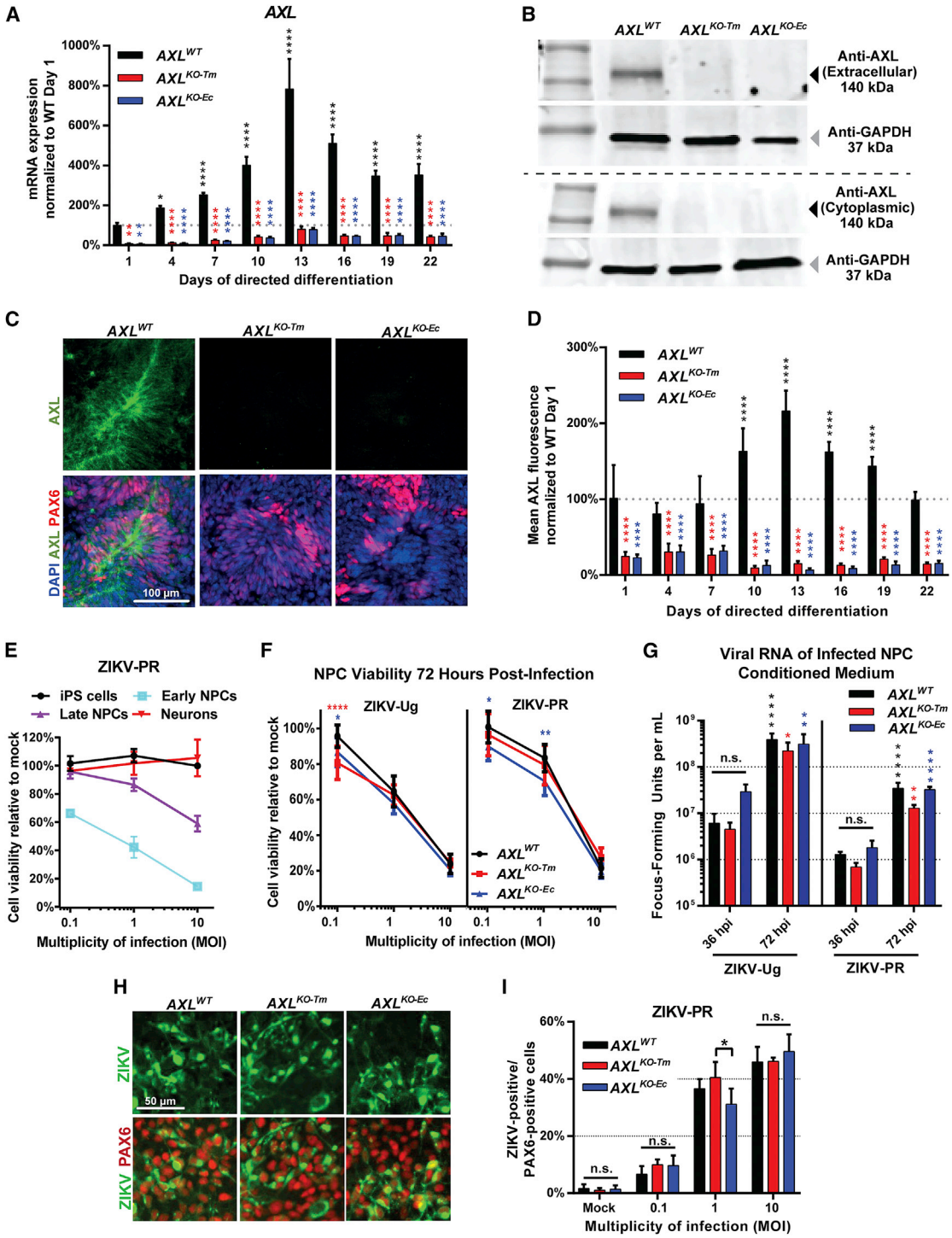

Figure 1. Loss of Human AXL Protein Does Not Protect NPCs from ZIKV Infection and Cell Death

(A) qRT-PCR analysis of *AXL* mRNA throughout NPC differentiation (n = 4). Black asterisks denote significance in AXL^{WT} compared to WT Day 1 values; red asterisks = AXL^{WT} versus $AXL^{KO\text{-}Tm}$ within time point; blue asterisks = AXL^{WT} versus $AXL^{KO\text{-}Ec}$ within time point.

(B) Western blot analysis confirms loss of AXL protein (140 kDa; black arrow head) in $AXL^{KO\text{-}Tm}$ and $AXL^{KO\text{-}Ec}$ NPCs using antibodies that target the extracellular and cytoplasmic domains of the protein. GAPDH, loading control.

(C) Representative fluorescent microscopy images of NPCs at Day 13 of the directed differentiation protocol. Images of $AXL^{KO\text{-}Tm}$ and $AXL^{KO\text{-}Ec}$ PAX6-positive NPCs confirm the absence of AXL protein.

(D) Quantification of immunofluorescent images indicates increased AXL expression during the NPC stage of directed differentiation and the absence of AXL protein in the $AXL^{KO\text{-}Tm}$ and $AXL^{KO\text{-}Ec}$ lines. Black asterisks denote significance in AXL^{WT} compared to WT Day 1 values; red asterisks = AXL^{WT} versus $AXL^{KO\text{-}Tm}$ within time point; blue asterisks = AXL^{WT} versus $AXL^{KO\text{-}Ec}$ within time point (n = 14 images from two wells per condition).

(legend continued on next page)

To allow study of the relationship between *AXL* expression, genotype, and differentiation state, we subjected *AXL* mutant and control iPSC lines to directed neuronal differentiation using inhibition of SMAD signaling (Chambers et al., 2009). Following neuralization, a time course of qRT-PCR measures of *AXL* mRNA abundance was performed from day 1 to 22. Only negligible levels of *AXL* transcript were found in the $AXL^{KO\text{-}Tm}$ and $AXL^{KO\text{-}Ec}$ differentiating cells at all time points ($p = 0.0018$; Figure 1A), suggesting that the induced mutations caused nonsense-mediated RNA decay. Western blotting using antibodies targeting the extracellular or cytoplasmic domains confirmed the loss of AXL protein in $AXL^{KO\text{-}Tm}$ and $AXL^{KO\text{-}Ec}$ NPCs (Figure 1B).

We next considered how the expression of *AXL* changed during neural differentiation of control iPSCs. We found an 8-fold increase in *AXL* expression between day 1 and the highest peak of expression at day 13 (AXL^{WT} Day 1 versus AXL^{WT} Day 13, $p < 0.0001$; Figure 1A). As differentiation proceeded (Day 22), *AXL* mRNA abundance declined (AXL^{WT} Day 13 versus AXL^{WT} Day 22, $p < 0.0001$; Figure 1A). Western blots confirmed this dynamic AXL expression pattern (AXL^{WT} Day 1 versus AXL^{WT} Day 13, $p = 0.0415$; Figure S1F). To determine if *AXL* was indeed expressed most prominently in NPCs, we co-stained differentiating cultures with antibodies recognizing AXL and the NPC transcription factor PAX6 (Figures 1C and 1D). These studies confirmed that AXL was present in control PAX6 progenitors and absent from $AXL^{KO\text{-}Tm}$ and $AXL^{KO\text{-}Ec}$ mutant NPCs. Importantly, expression analysis of the NPC marker *PAX6* (Figure S1G–S1I) showed that control and mutant iPSC lines generated PAX6-positive cells at comparable efficiencies.

To correlate ZIKV pathogenesis with *AXL* expression, we measured infectivity rates and cell death in different cell types infected with ZIKV originally isolated in Puerto Rico during the 2015 outbreak (ZIKV-PR). Supporting the importance of AXL in ZIKV cell entry in human lung A549 cells (Hamel et al., 2015), we found that siRNA knockdown of AXL reduced ZIKV-PR infectivity in A549 cells (Control versus AXL knockdown, $p = 0.024$; data not shown). We also found that iPSCs and post-mitotic neurons showed little to no ZIKV infectivity or cell death, consistent with previous reports (Tang et al., 2016) (Figure 1E). However, we found that early-stage NPCs (Day 21–35 of directed differentiation) were susceptible to ZIKV-PR in a dose-dependent manner, undergoing an 85% reduction in cell viability at a multiplicity of infection (MOI) of 10 when compared to mock-infected controls at 72 hr post-infection (hpi; Figure 1E).

We next compared the effects of ZIKV infection on early NPCs differentiated from the AXL^{WT}, $AXL^{KO\text{-}Tm}$, and $AXL^{KO\text{-}Ec}$ iPSC lines. When we infected these NPCs with either the original ZIKV strain isolated in Uganda in 1947 (ZIKV-Ug) or the modern ZIKV-PR strain at a range of MOIs (0.1, 1, or 10), we found a surprisingly comparable decrease in cell viability between genotypes, suggesting that ablation of *AXL* confers no protection from ZIKV-mediated cell death (Figure 1F). In fact, at the lowest MOI (0.1), $AXL^{KO\text{-}Tm}$ and $AXL^{KO\text{-}Ec}$ NPCs showed a modest but significant increase in viral-mediated cell death (ZIKV-Ug AXL^{WT} versus $AXL^{KO\text{-}Tm}$, $p < 0.0001$; ZIKV-Ug AXL^{WT} versus $AXL^{KO\text{-}Ec}$, $p = 0.021$; ZIKV-PR AXL^{WT} versus $AXL^{KO\text{-}Ec}$, $p = 0.028$). We then infected early NPCs with ZIKV-Ug or ZIKV-PR (MOI = 1) and collected conditioned media from each well at 36 hpi and 72 hpi for qRT-PCR to quantify virus present in the media. When we compared NPCs derived from all three iPSC lines, we found similar levels of ZIKV-Ug and ZIKV-PR RNA among the three genotypes (Figure 1G). To test whether AXL might function at the level of production of infectious ZIKV particles, we used conditioned media collected from AXL^{WT}, $AXL^{KO\text{-}Tm}$, and $AXL^{KO\text{-}Ec}$ NPCs at 72 hpi and administered it to Vero cells. Regardless of the *AXL* genotype of NPCs from which conditioned media was collected, near 100% secondary infectivity was observed (Figures S1J and S1K). Finally, we compared the infectivity rates of NPCs of the three *AXL* genotypes by quantifying the percentage of PAX6-positive cells that contained the ZIKV-PR envelope protein and found no differences between the wild-type and knockout early NPCs (Figures 1H and 1I) or late-stage radial glia-like NPCs (Day 36–45 of directed differentiation; data not shown).

To investigate the role of AXL in ZIKV-induced cell death in a model that closely mimics early human brain development, we generated 3D cerebral organoids from AXL^{WT} and $AXL^{KO\text{-}Tm}$ iPSCs (Figure 2A). By Day 24 of differentiation, organoids expressed phospho-vimentin, a marker of radial glia, in highly organized ventricle-like structures as revealed by light sheet microscopy (Figure S2A). We infected the organoids at MOI = 0.1, 1, and 10 on Day 24 with ZIKV-PR. Immunohistochemistry of fixed ZIKV-PR-infected organoid slices confirmed the presence of viral envelope protein in cells with a radial glial morphology that had organized into continuous neuroepithelial structures, as indicated by a rosette morphology and the presence of apical proliferation as determined by Ki67 staining (Figures 2B and 2C). These infected cells were observed in both the AXL^{WT} and $AXL^{KO\text{-}Tm}$ iPSC-derived cerebral organoids, demonstrating that elimination of AXL was not protective. When the cross-sectional size of the organoids was analyzed at 72 hpi, we found that while mock-infected AXL^{WT} organoids showed a 37% increase from their 0 hpi size, ZIKV-PR infected organoids (MOI = 10) increased

(E) ZIKV-PR infection (MOI = 0.1, 1, and 10) resulted in a dose-dependent decrease in the cell viability of early-stage NPCs and late-stage radial-glia-like NPCs, but not iPSCs and neurons, 72 hr post-infection (n = 8 wells).

(F) Loss of AXL protein did not protect NPCs from ZIKV-Ug-mediated or ZIKV-PR-mediated cell death (n = 8 wells). Red asterisks = AXL^{WT} versus $AXL^{KO\text{-}Tm}$; blue asterisks = AXL^{WT} versus $AXL^{KO\text{-}Ec}$.

(G) Quantification of ZIKV-Ug and ZIKV-PR viral RNA from conditioned media of infected (MOI = 1) AXL^{WT}, $AXL^{KO\text{-}Tm}$, and $AXL^{KO\text{-}Ec}$ NPCs at 36 hpi and 72 hpi (n = 6 wells).

(H) Representative images of AXL^{WT}, $AXL^{KO\text{-}Tm}$, and $AXL^{KO\text{-}Ec}$ early-stage NPCs infected with ZIKV-PR (MOI = 1). PAX6, red, NPC marker; 4G2, green, ZIKV envelope.

(I) Quantification of ZIKV-PR (MOI = 0.1, 1, and 10) infectivity of early-stage NPCs.

Two-way ANOVA (A, D, F, G, and I) with Tukey's multiple comparison tests was used for analysis: *$p < 0.05$, **$p < 0.01$, ****$p < 0.0001$, n.s. = not significant. Mean ± SD.

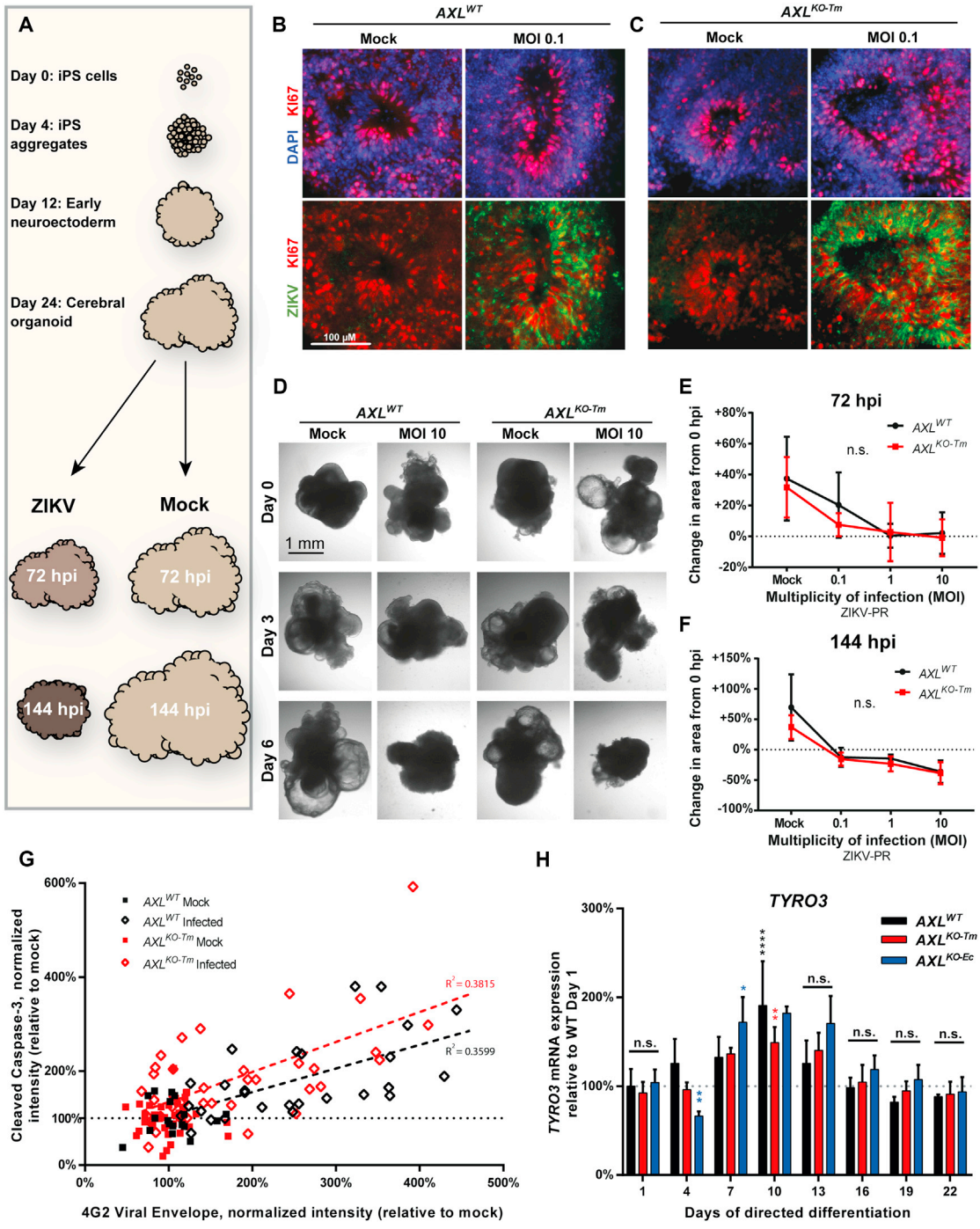

Figure 2. Knockout of Human AXL Does Not Prevent ZIKV Infection and Cell Death in Cerebral Organoids

(A) Schematic depicting the production of cerebral organoids from iPSC starting material. Cerebral organoids were infected with ZIKV-PR (MOI = 0.1, 1, and 10) at Day 24 and measured at Days 27 and 30.

(B and C) Immunohistochemistry of cryosectioned organoids 6 days after infection. Large, continuous neuroepithelial structures contained high levels of ZIKV-PR in both the (B) AXL^{WT} and (C) $AXL^{KO\text{-}Tm}$ cerebral organoids.

(D) Representative bright field images of mock and ZIKV-PR-infected (MOI = 10) AXL^{WT} and $AXL^{KO\text{-}Tm}$ cerebral organoids. Images were collected immediately following infection (Day 0), as well as 3 and 6 days post-infection.

(E and F) Quantification of cross-sectional organoid size at (E) 72 hpi and (F) 144 hpi. Over this time, mock-treated AXL^{WT} and $AXL^{KO\text{-}Tm}$ organoids increased in size while ZIKV-PR-infected organoids from both genotypes decreased in size. Data are presented as change in size compared to the size at time of infection (0 hpi) (n = 6 for each condition).

(G) Quantification of mock and infected (MOI = 0.1) organoid cryosections shows an increase in cleaved caspase-3 in response to increased viral presence. Samples were taken each day after infection for 8 days, and data shown is an aggregate of all time points. Each point represents the average cleaved caspase-3

(legend continued on next page)

by only 2% (Figures 2D and 2E). By 144 hpi, mock-infected AXL^{WT} organoid size increased 70% over this time course, while infected organoid size decreased by 36% (Figure 2F). Elimination of AXL did not protect cerebral organoids from the effects of infection, as $AXL^{KO\text{-}Tm}$ organoids exhibited a similar reduction in growth. We also found a correlation between the presence of the apoptotic marker cleaved caspase-3 and the presence of viral envelope protein in both the AXL^{WT} and $AXL^{KO\text{-}Tm}$ organoids (AXL^{WT} R^2 = 0.3599; $AXL^{KO\text{-}Tm}$ R^2 = 0.3815; Figure 2G, Figure S2B). Thus we conclude that ablation of AXL does not confer protection against ZIKV-PR in 2D NPC culture or 3D cerebral-organoid culture.

As removal of AXL was insufficient to inhibit ZIKV entry or cell death in NPCs, we considered the expression of additional candidate attachment factors. Analysis of gene expression in differentiating stem cells (Yao et al., 2017) revealed that in addition to *AXL* (Figure S2C), the candidate attachment factor *TYRO3* was expressed in NPCs (Figure S2D). In contrast, the additional candidate flavivirus attachment factors *DC-SIGN*, *TIM1*, and *TIM4* showed little to no expression in this cell type (Figure S2E). While qRT-PCR analysis revealed that *TYRO3* expression peaked at roughly twice that of iPSC levels at Day 10 before decreasing (Day 1 versus Day 10, $p < 0.0001$; Figure 2I), expression levels were also high in iPSCs, which are relatively recalcitrant to infection. There was no persistent difference in *TYRO3* expression between mutant *AXL* and control iPSC NPCs, suggesting that these cells did not further induce *TYRO3* expression as a compensatory mechanism in response to reduced *AXL* levels.

Our findings indicate that AXL is not essential for ZIKV infection of human NPCs and suggest that therapeutic inhibition of AXL alone would likely not be sufficient to mitigate ZIKV pathogenesis in developing brain tissue. Other studies have recently called into question the role of AXL in ZIKV infection of neural cell types. Multiple retinal cell types in *Axl* knockout mice ($Axl^{-/-}$) were not protected from ZIKV infection in vivo and ZIKV RNA levels in the brains of infected $Axl^{-/-}$ mice were comparable to that of wild-type animals, though the cell type specificity of infection was not investigated (Miner et al., 2016). Given the lack of protection conferred by the genetic ablation of *AXL*, further inquiries into potential ZIKV attachment factors in human NPCs, such as *TYRO3*, are needed. Overexpression of TYRO3 in HEK293 cells rendered this normally resistant cell type susceptible to ZIKV infection (Hamel et al., 2015). Interestingly, *TYRO3* expression is low or absent in A549 and HeLa cells (http://www.proteinatlas.org/ENSG00000092445-TYRO3/cell), which could explain why disruption of *AXL* is sufficient to significantly reduce ZIKV infectivity in these cells. Given that human NPCs co-express *AXL* and *TYRO3* (Onorati et al., 2016), it is possible that the targeted inhibition of both receptors might be required to protect these cells from ZIKV infection. It should be noted, however, that ZIKV-resistant iPSCs express relatively high levels of *TYRO3* (>50 TPM), calling into reasonable question the potential role of this protein in viral attachment. Efforts to identify the factors involved in ZIKV pathogenesis of human NPCs, through both targeted TAM receptor knockout studies and unbiased screening for factors that render NPCs resistant to ZIKV, will shed light on ZIKV tropism and lead to new therapeutic targets to protect against ZIKV infection.

SUPPLEMENTAL INFORMATION

Supplemental Information for this article includes two figures, two tables, and Supplemental Experimental Procedures and can be found with this article online at http://dx.doi.org/10.1016/j.stem.2016.11.011.

AUTHOR CONTRIBUTIONS

M.F.W., M.R.S., A.K., and K.E. designed all experiments and wrote the manuscript. M.F.W. and M.R.S. conducted and analyzed all ZIKV infections. K.A.W., R.J.I., and S.K. developed dox-iCas9 iPSCs and B.B. provided assistance with differentiation. M.R.S. established knockout lines. D.J.H. and C.Y. conducted NGS analysis. M.F.W., O.W., and E.J.H differentiated NPCs. J.R.K., E.J.H., and L.T.K. performed western blots.

ACKNOWLEDGMENTS

We thank Maura E. Charlton and Sid Paula for their assistance in safely acquiring the ZIKV at the initiation of this project as well as Kiki Lilliehook for reviewing the manuscript. We thank Priscilla L. Yang and Dominique J. Burri of Harvard Medical School for their help with propagating and quantifying ZIKV. We would also like to thank Nathaniel D. Kirkpatrick for imaging assistance and Ricardo E. Dolmetsch and Don E. Ganem for their guidance. K.E. was supported by the Stanley Center for Psychiatric Research and the Harvard Stem Cell Institute.

Received: September 20, 2016
Revised: November 4, 2016
Accepted: November 14, 2016
Published: December 1, 2016

REFERENCES

Brasil, P., Pereira, J.P., Jr., Raja Gabaglia, C., Damasceno, L., Wakimoto, M., Ribeiro Nogueira, R.M., Carvalho de Sequeira, P., Machado Siqueira, A., Abreu de Carvalho, L.M., Cotrim da Cunha, D., et al. (2016). Zika Virus Infection in Pregnant Women in Rio de Janeiro - Preliminary Report. N. Engl. J. Med., in press. Published online March 4, 2016. http://dx.doi.org/10.1056/NEJMoa1602412.

Brault, J.B., Khou, C., Basset, J., Coquand, L., Fraisier, V., Frenkiel, M.P., Goud, B., Manuguerra, J.C., Pardigon, N., and Baffet, A.D. (2016). Comparative Analysis Between Flaviviruses Reveals Specific Neural Stem Cell Tropism for Zika Virus in the Mouse Developing Neocortex. EBioMedicine *10*, 71–76.

Cao-Lormeau, V.M., Blake, A., Mons, S., Lastère, S., Roche, C., Vanhomwegen, J., Dub, T., Baudouin, L., Teissier, A., Larre, P., et al. (2016). Guillain-Barré Syndrome outbreak associated with Zika virus infection in French Polynesia: a case-control study. Lancet *387*, 1531–1539.

and 4G2 viral envelope fluorescence within a single rosette, normalized to the average fluorescence of mock-infected samples (n > 18 rosettes for each condition). Black linear regression represents AXL^{WT} with p = 0.00094 and red linear regression represents $AXL^{KO\text{-}Tm}$ with p = 0.000028.
(H) qRT-PCR analysis of *TYRO3* in AXL^{WT}, $AXL^{KO\text{-}Tm}$, and $AXL^{KO\text{-}Ec}$ cells over the course of 22 days of SMAD-inhibition differentiation. In unedited cells, the variation of *TYRO3* expression during differentiation was less severe than *AXL*, with peak expression occurring slightly earlier at Day 10 (n = 4). Vertically arranged black asterisks denote significance in AXL^{WT} compared to WT Day 1 values. Red asterisks = AXL^{WT} versus $AXL^{KO\text{-}Tm}$ within time point; blue asterisks = AXL^{WT} versus $AXL^{KO\text{-}Ec}$ within time point. Two-way ANOVA (E, F, and H) with Tukey's multiple comparison tests was performed: *p < 0.05, **p < 0.01, ****p < 0.0001, n.s. = not significant. Mean ± SD.

Chambers, S.M., Fasano, C.A., Papapetrou, E.P., Tomishima, M., Sadelain, M., and Studer, L. (2009). Highly efficient neural conversion of human ES and iPS cells by dual inhibition of SMAD signaling. Nat. Biotechnol. *27*, 275–280.

Cugola, F.R., Fernandes, I.R., Russo, F.B., Freitas, B.C., Dias, J.L., Guimarães, K.P., Benazzato, C., Almeida, N., Pignatari, G.C., Romero, S., et al. (2016). The Brazilian Zika virus strain causes birth defects in experimental models. Nature *534*, 267–271.

Dang, J., Tiwari, S.K., Lichinchi, G., Qin, Y., Patil, V.S., Eroshkin, A.M., and Rana, T.M. (2016). Zika Virus Depletes Neural Progenitors in Human Cerebral Organoids through Activation of the Innate Immune Receptor TLR3. Cell Stem Cell *19*, 258–265.

Garcez, P.P., Loiola, E.C., Madeiro da Costa, R., Higa, L.M., Trindade, P., Delvecchio, R., Nascimento, J.M., Brindeiro, R., Tanuri, A., and Rehen, S.K. (2016). Zika virus impairs growth in human neurospheres and brain organoids. Science *352*, 816–818.

Hamel, R., Dejarnac, O., Wichit, S., Ekchariyawat, P., Neyret, A., Luplertlop, N., Perera-Lecoin, M., Surasombatpattana, P., Talignani, L., Thomas, F., et al. (2015). Biology of Zika Virus Infection in Human Skin Cells. J. Virol. *89*, 8880–8896.

Hunt, C.L., Kolokoltsov, A.A., Davey, R.A., and Maury, W. (2011). The Tyro3 receptor kinase Axl enhances macropinocytosis of Zaire ebolavirus. J. Virol. *85*, 334–347.

Malkki, H. (2016). CNS infections: Zika virus infection could trigger Guillain-Barré syndrome. Nat. Rev. Neurol. *12*, 187.

Meertens, L., Carnec, X., Lecoin, M.P., Ramdasi, R., Guivel-Benhassine, F., Lew, E., Lemke, G., Schwartz, O., and Amara, A. (2012). The TIM and TAM families of phosphatidylserine receptors mediate dengue virus entry. Cell Host Microbe *12*, 544–557.

Miner, J.J., Sene, A., Richner, J.M., Smith, A.M., Santeford, A., Ban, N., Weger-Lucarelli, J., Manzella, F., Rückert, C., Govero, J., et al. (2016). Zika Virus Infection in Mice Causes Panuveitis with Shedding of Virus in Tears. Cell Rep. *16*, 3208–3218.

Mlakar, J., Korva, M., Tul, N., Popović, M., Poljšak-Prijatelj, M., Mraz, J., Kolenc, M., Resman Rus, K., Vesnaver Vipotnik, T., Fabjan Vodušek, V., et al. (2016). Zika Virus Associated with Microcephaly. N. Engl. J. Med. *374*, 951–958.

Nowakowski, T.J., Pollen, A.A., Di Lullo, E., Sandoval-Espinosa, C., Bershteyn, M., and Kriegstein, A.R. (2016). Expression Analysis Highlights AXL as a Candidate Zika Virus Entry Receptor in Neural Stem Cells. Cell Stem Cell *18*, 591–596.

Oehler, E., Watrin, L., Larre, P., Leparc-Goffart, I., Lastere, S., Valour, F., Baudouin, L., Mallet, H., Musso, D., and Ghawche, F. (2014). Zika virus infection complicated by Guillain-Barre syndrome–case report, French Polynesia, December 2013. Euro Surveill. *19*, 19.

Onorati, M., Li, Z., Liu, F., Sousa, A.M., Nakagawa, N., Li, M., Dell'Anno, M.T., Gulden, F.O., Pochareddy, S., Tebbenkamp, A.T., et al. (2016). Zika Virus Disrupts Phospho-TBK1 Localization and Mitosis in Human Neuroepithelial Stem Cells and Radial Glia. Cell Rep. *16*, 2576–2592.

Petersen, E.E., Staples, J.E., Meaney-Delman, D., Fischer, M., Ellington, S.R., Callaghan, W.M., and Jamieson, D.J. (2016). Interim Guidelines for Pregnant Women During a Zika Virus Outbreak–United States, 2016. MMWR Morb. Mortal. Wkly. Rep. *65*, 30–33.

Qian, X., Nguyen, H.N., Song, M.M., Hadiono, C., Ogden, S.C., Hammack, C., Yao, B., Hamersky, G.R., Jacob, F., Zhong, C., et al. (2016). Brain-Region-Specific Organoids Using Mini-bioreactors for Modeling ZIKV Exposure. Cell *165*, 1238–1254.

Rubin, E.J., Greene, M.F., and Baden, L.R. (2016). Zika Virus and Microcephaly. N. Engl. J. Med. *374*, 984–985.

Sarno, M., Sacramento, G.A., Khouri, R., do Rosário, M.S., Costa, F., Archanjo, G., Santos, L.A., Nery, N., Jr., Vasilakis, N., Ko, A.I., and de Almeida, A.R. (2016). Zika Virus Infection and Stillbirths: A Case of Hydrops Fetalis, Hydranencephaly and Fetal Demise. PLoS Negl. Trop. Dis. *10*, e0004517.

Savidis, G., McDougall, W.M., Meraner, P., Perreira, J.M., Portmann, J.M., Trincucci, G., John, S.P., Aker, A.M., Renzette, N., Robbins, D.R., et al. (2016). Identification of Zika Virus and Dengue Virus Dependency Factors using Functional Genomics. Cell Rep. *16*, 232–246.

Soares de Oliveira-Szejnfeld, P., Levine, D., Melo, A.S., Amorim, M.M., Batista, A.G., Chimelli, L., Tanuri, A., Aguiar, R.S., Malinger, G., Ximenes, R., et al. (2016). Congenital Brain Abnormalities and Zika Virus: What the Radiologist Can Expect to See Prenatally and Postnatally. Radiology *281*, 203–218.

Tang, H., Hammack, C., Ogden, S.C., Wen, Z., Qian, X., Li, Y., Yao, B., Shin, J., Zhang, F., Lee, E.M., et al. (2016). Zika Virus Infects Human Cortical Neural Progenitors and Attenuates Their Growth. Cell Stem Cell *18*, 587–590.

Yao, Z., Mich, J.K., Ku, S., Menon, V., Krostag, A.R., Martinez, R.A., Furchtgott, L., Mulholland, H., Bort, S., Fuqua, M.A., et al. (2017). A Single-Cell Roadmap of Lineage Bifurcation in Human ESC Models of Embryonic Brain Development. Cell Stem Cell *20*, in press. Published online October 27, 2016. http://dx.doi.org/10.1016/j.stem.2016.09.011.